Supplementary Information:

Dynamic stabilisation during the drainage of thin film polymer solutions

Emmanouil Chatzigiannakis and Jan Vermant*

Department of Materials, ETH Zürich,

Vladimir Prelog Weg 5, 8032 Zürich, Switzerland

(Dated: April 8, 2021)

---

*Electronic address: `jan.vermant@mat.ethz.ch`

S I. GPC RESULTS

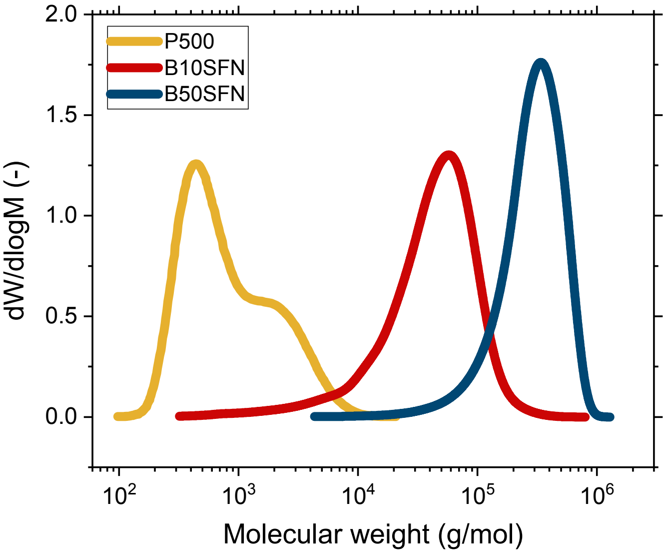

Fig. S 1: The molecular weight distributions of the polyisobutylene grades used in this study as obtained by GPC.

Table S I: Molecular characteristics of the polyisobutylenes as obtained by GPC

Polyisobutylene grade	M_w [g/mol]	M_n [g/mol]	M_z [g/mol]	PDI [-]
P500	1273	599	3100	2.13
B10SFN	54464	19619	86513	2.78
B50SFN	327079	212516	409173	1.54

S II. DRAINAGE OF THIN LIQUID FILMS

The main observables from a DTFB experiments is (i) the coalescence time and (ii) the thickness and (iii) the radius evolution of the film. In this section we report our findings with respect to these three parameters. In most of the cases our results agree with previously published simulation results and theoretical predictions [1–3]. To the best of our knowledge, this is the first reporting of experimental results from direct film drainage observations at various *Ca* numbers.

As discussed in section 4.1, the coalescence time of the four solutions of the medium Mw polymer were found to depend linearly on viscosity, as expected from the Reynolds equation. This can be clearly seen in Fig. 2a, where we plot the reduced coalescence time, t_c/η as a function of the applied pressure drop. The curves of the four solutions overlap, showing the expected for pressure-driven flow $t_c \propto \Delta P^{-1}$ relation at high ΔP. The relatively poorer overlap that can be observed at low ΔP, which however is still within experimental error, can be attributed to the stochasticity of the rupture process at low Ca [4] and to the different number of conducted measurements among samples.

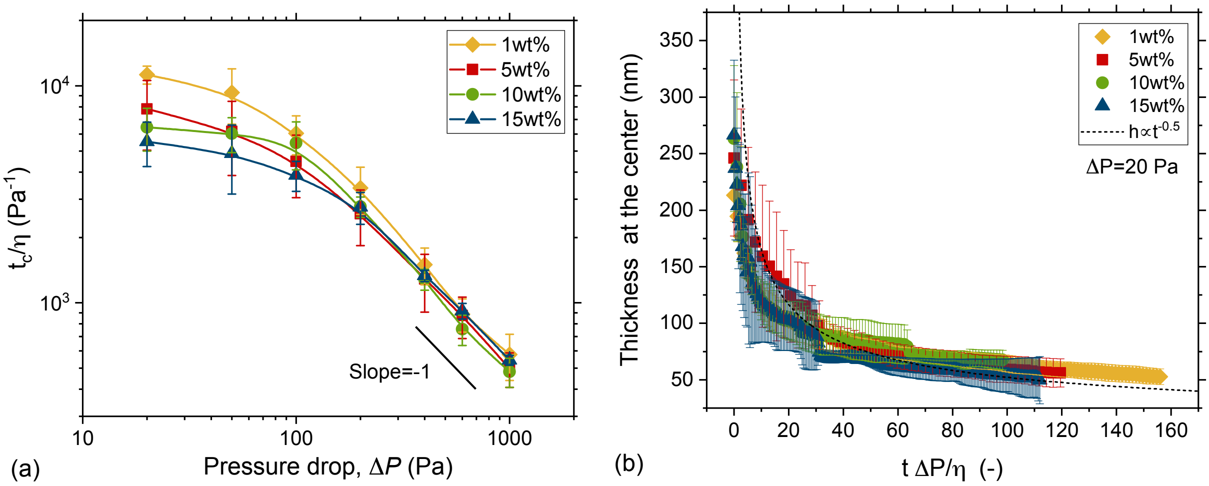

Fig. S 2: (a) The reduced drainage time as a function of the applied pressure drop for the solutions of the medium Mw polymer. (b) The drainage curves of the same solutions as a function of the dimensionless time (average of three measurements). The expected dependencies based on the Reynolds equation are shown in both graphs.

The drainage curves, i.e. the thickness evolution over time, of all films also followed the expected viscosity dependence. In Fig. 2b we plot the measured average thickness at the centre of the film as a function of the dimensionless time $t\Delta P/\eta$ for the lowest applied pressure drop of 20 Pa. The large error bars and the step-decreases in thickness are attributed to the occurrence of instabilities, as discussed in the main article. The decrease in thickness followed the $h \propto t^{-1/2}$ relation that is predicted from the Reynolds equation for planar films (shown as a dashed line). This relation does not hold for dimpled films draining at higher Ca numbers [5, 6].

The radius of the film at equilibrium is controlled by the pressure balance at the Plateau border [7, 8]:

$$\frac{2\sigma}{R} + \Delta P = \frac{2\sigma R}{R^2 - R_f^2} \tag{1}$$

where R is the radius of the bike-wheel's hole and R_f the radius of the film. In Eq. 1 the effect of contact angles has been neglected. Upon the application of the extra ΔP the film will expand until the equilibrium film radius is reached. The median film expansion rates for all pressure drops are shown for the 5 wt% solution films in Fig. 3a. The determination of the radii starts at the onset of drainage, t_0 and stops at film rupture (t_c). In Fig. 3b we plot the median dimensionless radius R_f/R as a function of the dimensionless time. All curves overlap showing that the expansion of the film is also controlled by viscosity. Moreover, the dimensionless radius increased with $t^{1/2}$. The radii of the films just before rupture have been found to agree with Eq. 1, which can be approximated as $R \propto Ca^{1/2}$ [3], and can be found in an earlier publication of our group [9].

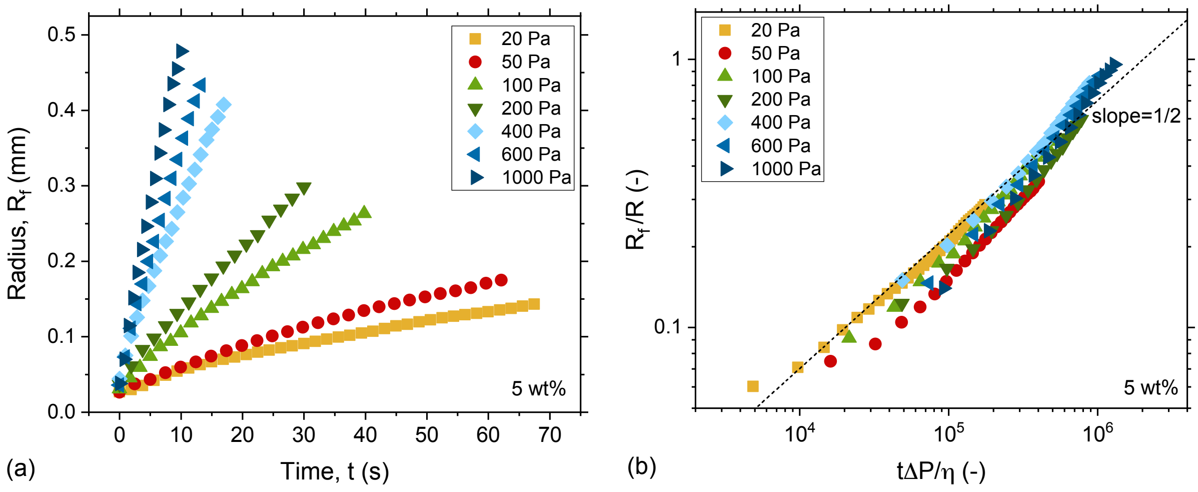

Fig. S 3: (a) The evolution of film radius with time for different pressure drops ΔP. for the 5 wt% solution. The radius is measured using the first change in the order of interference as a limit until rupture occurs. (b) The dimensionless film radius R/R_f as a function of dimensionless time. A dependence of $R/R_f \propto (t\Delta P/\eta)^{1/2}$ is observed for all pressure drops.

In Fig. 4a we plot the average film expansion rate (assumed to be equal to $R_f|_{t=t_c}/t_c$) as a function of applied pressure drop for all solutions of the medium Mw polymer. The average dR_f/dt increased linearly with pressure drop ΔP justifying our choice of using dR_f/dt as the characteristic velocity of drainage for the estimation of the Péclet number. Moreover, dividing the applied pressure drop by the bulk viscosity of the solutions resulted in an excellent overlap for the expansion curves of all solutions (Fig. 4b).

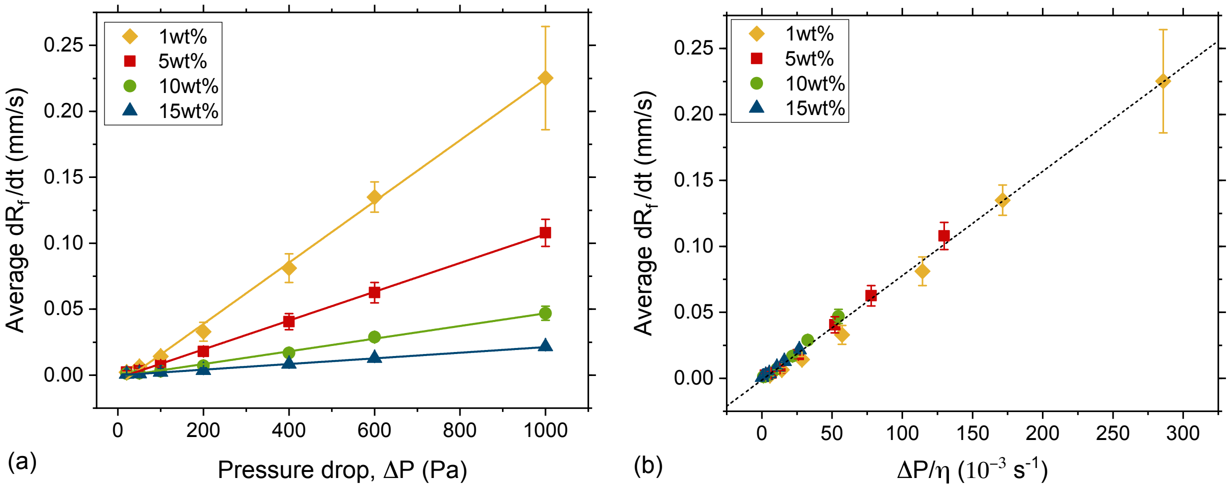

Fig. S 4: (a) The average film expansion rate as a function of applied ΔP for all the solutions of the medium Mw polymer. (b) The same average expansion rates as a function of the reduced pressure drop $\Delta P/\eta$.

The average maximum thickness at rupture is shown as a function of ΔP in Fig. 5a for the solutions of the medium Mw polymer. If drainage is symmetric, then the maximum thickness corresponds to the centre of the dimple. In contrast, if drainage is asymmetric, then the maximum thickness corresponds to the highest point observed in vortices or channels. The maximum thickness was found to increase approximately as $h_{max} \propto \Delta P$. The lower h_{max} of the 5 wt% solution is related to its propensity for instabilities.

Finally, the average thickness h_{avg} of the medium Mw polymer solution films is shown as a function of ΔP in Fig. 5b. h_{avg} is determined by the thickness profiles in the radial direction assuming axisymmetry $h_{avg} = \int_{-R}^{R} h(r)dr$. An approximate relation of $h_{avg} \propto \Delta P^{0.5}$ was observed. The volume of the film, calculated from $V = \pi R_f^2 h_{avg}$ increased linearly with ΔP (Fig. 5c).

S III. OSMOTIC STRESSES

A. Estimation of osmotic pressure, Os_{st}, and Os_d

In this section we provide a detailed description of the method used to estimate the static (Os_{st}) and dynamic (Os_d) dimensionless numbers.

The osmotic pressure of polymer solutions was approximated using a virial expansion as [10]:

$$\Pi_{osm} = \frac{\bar{R}Tc}{M_n}\left(1+A_2^*\frac{M_n c}{2}\right)^2 \quad , \tag{2}$$

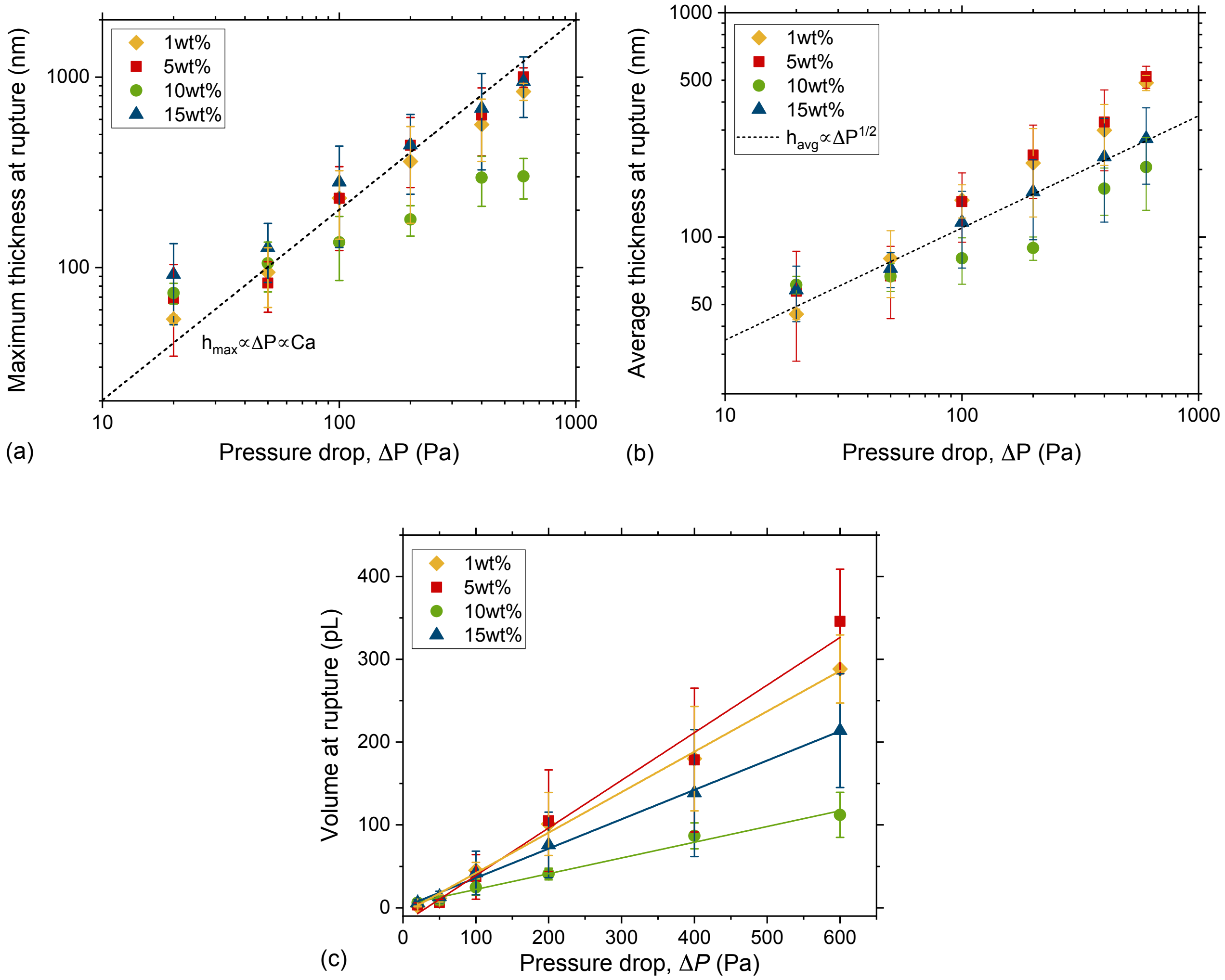

Fig. S 5: (a) The maximum thickness of the medium Mw solution films as a function of ΔP. (b) The volume of the films as a function of ΔP.

where c is the concentration, M_n is the number-average molecular weight (the osmotic pressure is a colligative property [11]), $\bar{R}$ is the gas constant, and A_2^* is an effective concentration-dependent virial coefficient, equal to:

$$A_2^* = \frac{16\pi N_0 [\eta]}{M_n \left[9.3 \cdot 10^{24} + 4\pi N_0 c \left([\eta] - [\eta]_\theta\right)\right]} \left(1 - \frac{[\eta]_\theta}{[\eta]}\right) \quad , \tag{3}$$

where $[\eta]$ is the intrinsic viscosity, $[\eta]_\theta$ is the intrinsic viscosity in a θ-solvent, and N_0 is the Avogadro number. Eq. 2 can qualitatively describe the increase in the osmotic pressure that is expected for polymer solutions above c^* [12]. As mentioned above, when concentration differences Δc are present, these will result in osmotic pressure differences $\Delta\Pi_{osm}$. Eq. 2 indicates that the magnitude of the lateral osmotic stresses between a depleted and a concentrated region will be different for a given Δc when the initial concentration is close to c^*.

The calculated static and dynamic osmotic numbers using the literature values [13] of $[\eta]$ and $[\eta]_\theta$ and the experimentally determined M_n are shown in Fig. 6a and 6b, respectively.

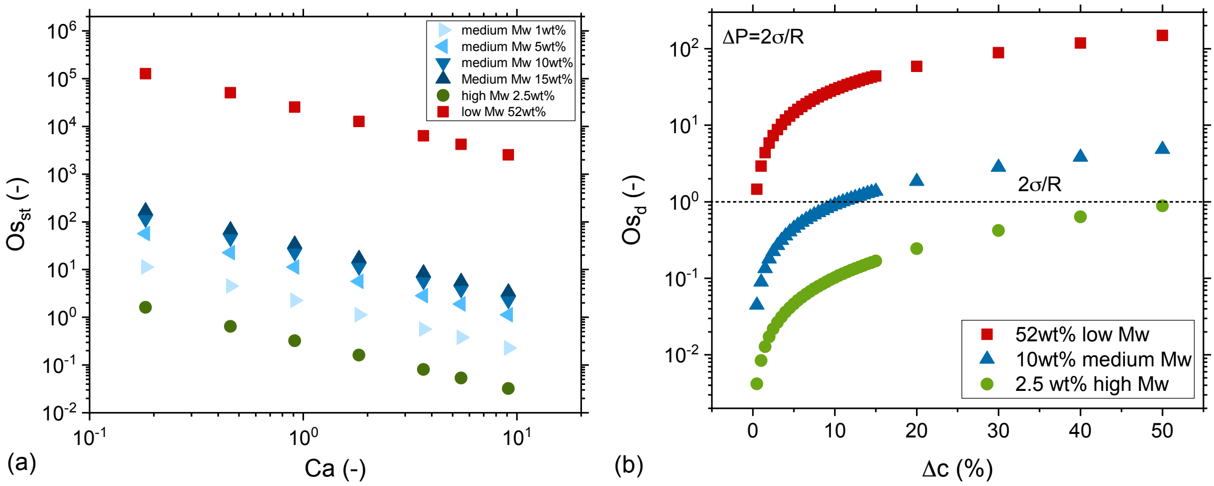

Fig. S 6: (a) The calculated static osmotic number for all polymer solutions as a function of the Ca number. (b) The dynamic osmotic number for solutions of the same bulk viscosity but different molecular weight at a pressure drop $\Delta P = 2\sigma/R$ as a function of concentration differences.

B. Supplementary experimental results

The lateral organisation that was observed in some films of the highest concentration solutions of the medium Mw is shown in Fig. 7. The structuring of the confined polymer molecules resulted in thickness steps in the radial direction.

The period of instabilities for the low Mw polymer solutions are shown in Fig. 8. An exponent a between 1/2 and 1 was observed for $T_f \propto Os_d^a$, in agreement to the scaling relations discussed in the main article. The higher standard deviation in the determined periods is due to the lower number of measurements conducted for the lower Mw samples.

The stabilising effect of capillarity, as described by the Ca number is shown in Fig. 9 for the films of the medium Mw solution. The probability for the occurrence of instabilities follows a normal cumulative distribution, with the Ca number promoting axisymmetric drainage. The only notable exception is the 10 wt% solution (close to c^*), which as discussed in the main text shows

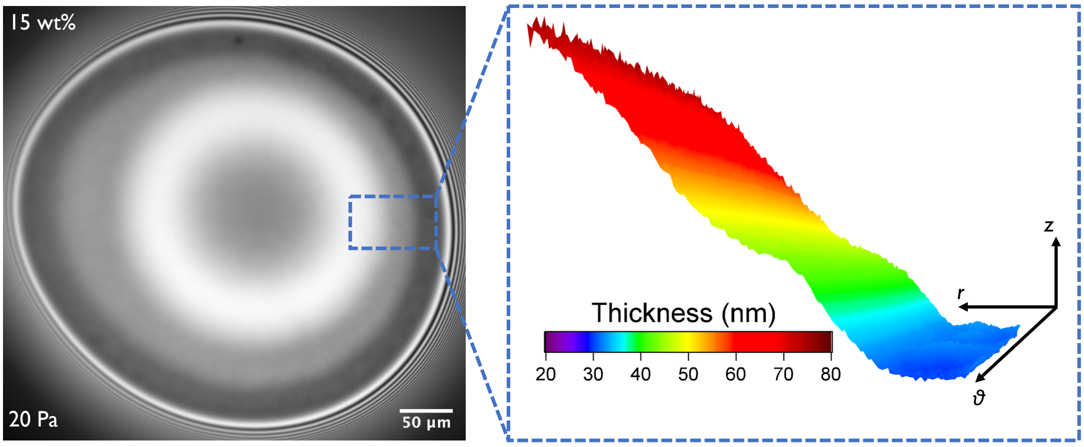

Fig. S 7: The lateral organisation of polymer molecules in a film of a 15wt% solution of the medium Mw polymer ($\Delta P = 20\ Pa$). *Left*: Microinterferometry image of a film just before rupture. *Right*: 3D thickness plot of the marked area.

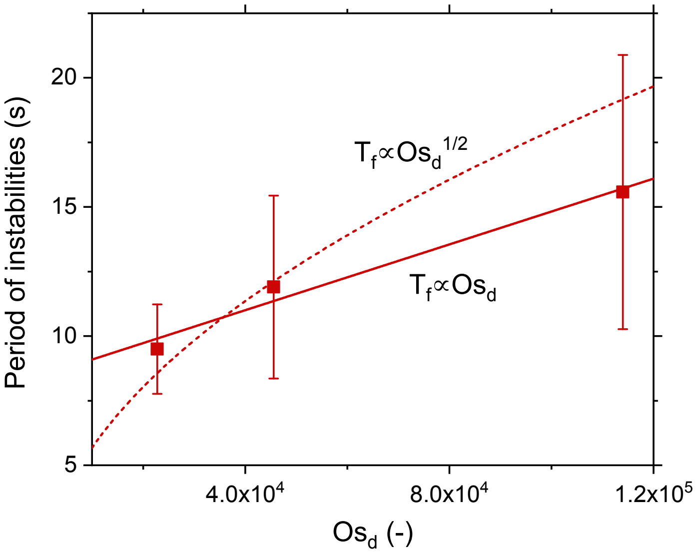

Fig. S 8: The characteristic timescale (or period of instabilities) as a function of the calculated dynamic osmotic number for the low Mw polymer solution.

a propensity for instabilities (shown in the blue area in Fig. 9).

In Fig. 10 we compare the critical or minimum thickness of the medium M_w solutions to that of the low M_w polymer as a function of ΔP. The critical thickness is, at least for the low ΔP, always related to the thickness of the dark spots). Despite the significantly different R_H of the two polymers, thickness values are the same within experimental error. This is another indication that the dark spots are depleted film regions that contain no polymer molecules, in agreement with the

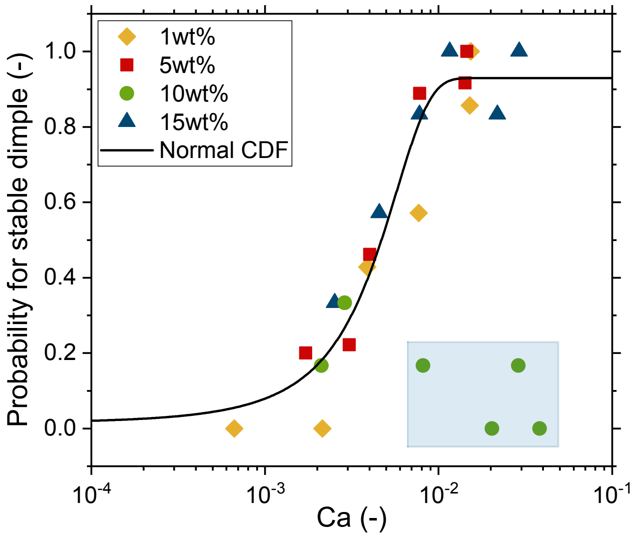

Fig. S 9: The probability of stable dimple as a function of the *a posteriori* calculated Ca number. The Ca number was calculated from Eq.3 of the main text using the experimentally determined characteristic velocities, radii, and thicknesses.

results of Sethumadhavan et al. on films containing nanoparticles [14]. The ability of the modified Vrij model [15] that considers the hydrodynamic dampening of fluctuations [4], to predict the increase in critical thickness, is also consistent with the break-up of films locally depleted of polymer.

S IV. FILM IMAGES

Selected film images as obtained by microinterferometry for the medium Mw polymer solutions at three different pressure drops (20, 200, and 1000 Pa) are shown in Fig. 11. All images correspond to films just before rupture.

S V. DRAINAGE MOVIES

Movie S1: A film of the low Mw polymer solution draining under $\Delta P = 50\ Pa$ (10x speed). The film is draining asymmetrically.

Movie S2: A film of the low Mw polymer solution draining under $\Delta P = 400\ Pa$ (2x speed). The film is draining symmetrically due to the stabilising effect of capillarity as ΔP increases.

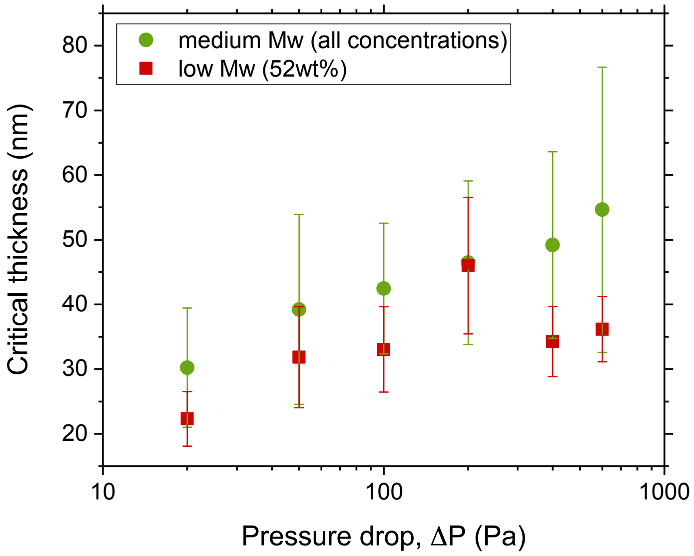

Fig. S 10: The critical thickness as a function of applied pressure drop for the low and medium Mw polymer solutions. The green circles are the average values of all polymer solutions of the medium Mw polymer, while the red squares correspond to the lom Mw at $c = 52\ wt\%$.

Movie S3: A film of the mixed solutions draining under $\Delta P = 50\ Pa$ (5x speed). The film is draining asymmetrically with the cyclic dimple formation being followed by channel drainage.

Movie S4: A film of the mixed solutions draining under $\Delta P = 200\ Pa$ (2x speed). The film is draining asymmetrically. The dimple wash-out is followed by the formation of vortices and the re-thickening of the dimple.

Movie S5: A film of the mixed solutions draining under $\Delta P = 400\ Pa$ (2x speed). Drainage is highly asymmetric.

Movie S6: A film of the mixed solutions draining under $\Delta P = 1000\ Pa$ (2x speed). Drainage is highly asymmetric with the size of vortices having increased compared to movie S5.

Movie S7: A film of the mixed solutions draining under $\Delta P = 100\ Pa$ (5x speed). The dimple wash-out is followed by dimple reformation, recoil, and thickening.

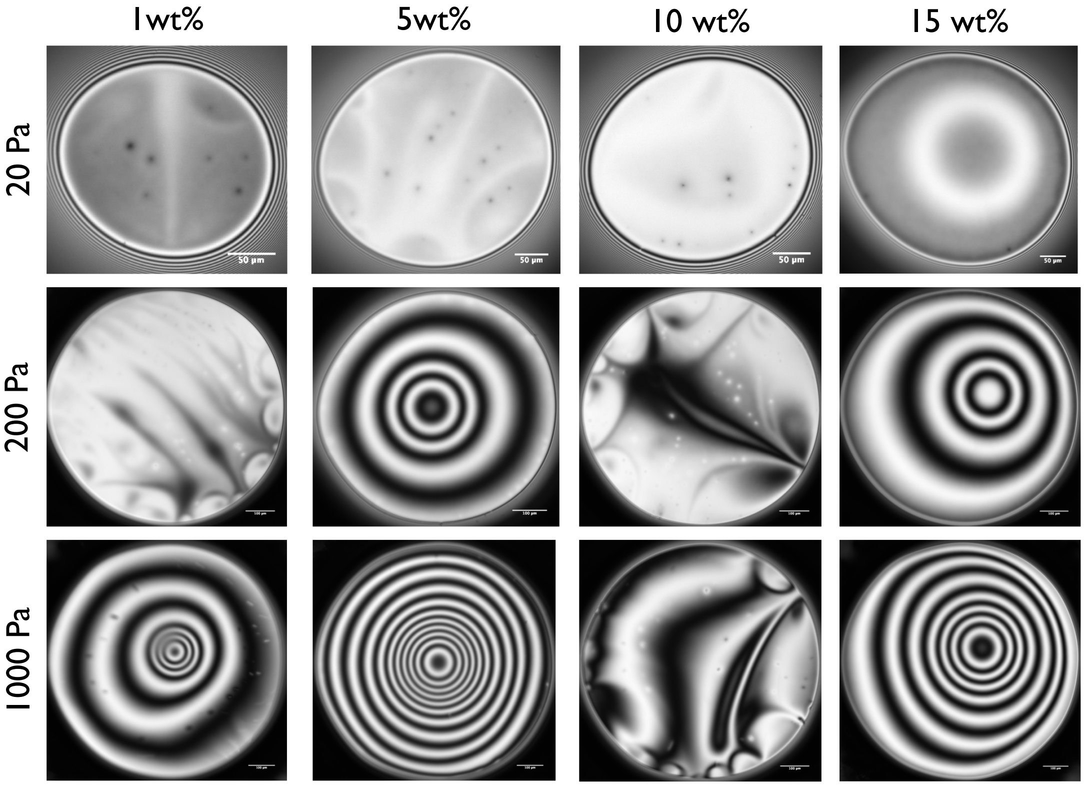

Fig. S 11: Films just before rupture for the four studied concentrations of the medium Mw polymer solutions. Three different pressure drops ΔP are shown. The propensity of the 10 wt% solution for instabilities is evident. When drainage is symmetric, the size of the dimple increases with ΔP.

Movie S8: A film of the high Mw polymer solution draining under $\Delta P = 50\ Pa$ (5x speed). The film is draining symmetrically and a formation of a small dimple can be observed.

Movie S9: A film of the high Mw polymer solution draining under $\Delta P = 100\ Pa$ (2x speed). No dimple or thickness corrugations are observed.

Movie S10: A film of the high Mw polymer solution draining under $\Delta P = 100\ Pa$ (1x speed). No dimple or thickness corrugations are observed despite the high Ca number.

---

[1] P. Janssen, P. Anderson, G. Peters, and H. Meijer, Journal of Fluid Mechanics **567**, 65 (2006).

[2] F. Baldessari and L. G. Leal, Physics of fluids **18**, 013602 (2006).

[3] L. Leal, Physics of fluids **16**, 1833 (2004).

[4] E. Chatzigiannakis and J. Vermant, Physical Review Letters **125**, 158001 (2020).

[5] D. Y. Chan, E. Klaseboer, and R. Manica, Soft Matter **6**, 1809 (2010).

[6] E. Chatzigiannakis, N. Jaensson, and J. Vermant, Current Opinion in Colloid & Interface Science p. 101441 (2021).

[7] B. Toshev and I. Ivanov, Colloid and Polymer Science **253**, 558 (1975).

[8] S. Karakashev, Colloids and Surfaces A: Physicochemical and Engineering Aspects **372**, 151 (2010).

[9] E. Chatzigiannakis, P. Veenstra, D. ten Bosch, and J. Vermant, Soft Matter **16**, 9410 (2020).

[10] C. M. Kok and A. Rudin, Journal of Applied Polymer Science **26**, 3575 (1981).

[11] M. Rubinstein, R. H. Colby, et al., *Polymer physics*, vol. 23 (Oxford university press New York, 2003).

[12] R. H. Colby, Rheologica acta **49**, 425 (2010).

[13] W. Krigbaum and P. Flory, Journal of Polymer Science **11**, 37 (1953).

[14] G. N. Sethumadhavan, A. D. Nikolov, and D. T. Wasan, Journal of colloid and interface science **240**, 105 (2001).

[15] A. Vrij, Discussions of the Faraday Society **42**, 23 (1966).